

LA-UR-14-29095 (Accepted Manuscript)

Elasticity in Crystalline Molecular Explosives

Hooks, Daniel Edwin
Ramos, Kyle James
Bolme, Cynthia Anne
Cawkwell, Marc Jon

Provided by the author(s) and the Los Alamos National Laboratory (2016-02-18).

To be published in: PROPELLANTS EXPLOSIVES PYROTECHNICS ; Vol.40, iss.3, spec. iss.SI, p.333-350,
JUN 2015

DOI to publisher's version: 10.1002/prop.201400282

Permalink to record: <http://permalink.lanl.gov/object/view?what=info:lanl-repo/lareport/LA-UR-14-29095>

Disclaimer:

Approved for public release. Los Alamos National Laboratory, an affirmative action/equal opportunity employer, is operated by the Los Alamos National Security, LLC for the National Nuclear Security Administration of the U.S. Department of Energy under contract DE-AC52-06NA25396. Los Alamos National Laboratory strongly supports academic freedom and a researcher's right to publish; as an institution, however, the Laboratory does not endorse the viewpoint of a publication or guarantee its technical correctness.

Elasticity in Crystalline Molecular Explosives

Daniel E. Hooks*, Kyle J. Ramos, Cindy A. Bolme, Marc J. Cawkwell ^[a]

Abstract: Crystalline molecular explosives are key components of engineered explosive formulations. In precision applications a high degree of consistency and predictability is desired under a range of conditions to a variety of stimuli. Prediction of behaviors from mechanical response and failure, to detonation initiation, and ultimately the detonation performance of the material is tied to accurate knowledge of the material structure and first stage of deformation: elasticity. The elastic response of pentaerythritol tetranitrate (PETN), cyclotrimethylene trinitramine (RDX), and cyclotetramethylene tetranitramine (HMX), including aspects of material and measurement variability, and computational methods are described in detail. Experimental determinations of elastic tensors are compared, and an evaluation of sources of error is presented. Computed elastic constants are also compared for these materials and for triaminotrinitrobenzene (TATB), for which there are no measurements.

[a] D. E. Hooks, K. J. Ramos, C. A. Bolme, M. J. Cawkwell
Los Alamos National Laboratory
Los Alamos, NM 87545 USA
dhooks@lanl.gov

1 Introduction

Robert Hooke published his work describing the proportionality of force and distance in springs and solid materials in 1678.^[1] The adaptation of Hooke's Law, by Thomas Young in 1807,^[2] to describe material stress and strain with a simple proportionality constant, remains a fundamental area of study in materials. In explosives, it is both a starting point for first-principles models of solid behaviors and the link to plastic flow, failure, and chemical reaction, and an essential material property for the prediction of explosive performance in hydrodynamic states.

A crucial aspect of the performance and safety response of explosives relates to the translation of mechanical stimuli to chemical energy release. It has been known by theory and inferential experiments that material perturbations of many kinds may give rise to "hot spots" where energy localizes, resulting in increased temperatures and the onset of chemical reaction. The concept of energy localization, or hot spots, through several general mechanisms, including void collapse and friction along with other means was introduced in the 1940s.^{[3-5],[6]} Accurate constitutive relationships, incorporating elasticity and rate-dependent plasticity, are necessary to quantify the temperature distribution in the material surrounding these defects and understand the efficacy they have on initiation.^[7]

The compressibility of explosive material is also a factor in predicting the peak pressure achieved upon detonation.^[8-10] Accurate constitutive relationships provide constraints on reactant equation of state.^[11-14] The reactant bulk modulus and its pressure derivatives are commonly extrapolated to detonation pressures, and with the product equation of state, predict the peak detonation pressure and reaction zone.

In this article, we will focus on the common explosives pentaerythritol tetranitrate (PETN), cyclotrimethyltrinitramine (RDX), and cyclotetramethyltetranitramine (HMX), for

which much has been measured, predicted, and written over the past several decades. Given the increasing complexity of these three materials from the standpoint of crystal structure (tetragonal, orthorhombic, and monoclinic, respectively) and associated properties, it is instructive to evaluate information available for each, and how conclusions can be drawn across these materials and extrapolated to others. This is particularly important for low symmetry molecular materials, whose complexity makes physical measurement challenging. We will then extend to a comparison of predictions for triclinic triaminotrinitrobenzene (TATB), for which few property measurements have been made.

To evaluate the response of composite explosives to external stimuli, one must proceed through the four fundamental steps of solid mechanics: granular mechanics, elastic compression, plastic flow and failure, and phase transitions. Our focus is on elasticity for PETN, RDX, and HMX, and the evaluation of several types of measurement techniques, experimental results, and computational approaches. Given that crystal structure and simple compressibility is a fundamental check for models of materials, the accuracy of these measurements directly constrains the accuracy of predictions – especially where extrapolation is required. We will describe the potential sources of variability in elasticity measurement and associated predictions. Through review and analysis of available data, we will demonstrate the origin of much of the previous conflicting elasticity determinations and propose a path for increased accuracy in the future. We will also introduce new predictions of the elastic tensor of RDX and describe differences with experimental determinations and previous predictions for this and other materials.

1.1 Mechanics of Explosives Crystals

During manufacture and impact loading of composite explosives, the energetic molecular crystal constituent undergoes deformation, beginning with elastic deformation. The molecule, crystal structure, microstructure, and deformation mechanisms combine to determine sensitivity to detonation during dynamic compression. In order to control and improve safety and performance deformation processes must be understood. Although deformation has been extensively studied in a wide range of materials, ranging from metals to polymers, by comparison, deformation in molecular crystals has received relatively little attention.

PETN, RDX, and HMX are heavily used secondary explosives, with deformation behaviors studied in single crystal form and as-formulated, both quasi-statically and dynamically. Quasi-static and dynamic studies have explored microstructure, deformation mechanisms, Hugoniot elastic limits (HEL), polymorphic phase transformations, and initiation of detonation. Although these experiments have demonstrated the unique features of crystal mechanics and anisotropy, efforts to correlate static and dynamic effects, elastic and plastic deformation, defect contributions, and other factors with initiation has proven difficult.^[15-29] A major focus of ongoing work is direct, *in-situ* observation of microstructural phenomena and fundamental properties.^[30, 31] Initiation sensitivity in formulations is variable and dependent on impurities, microstructure, and formulation parameters. Initiation mechanisms are uncertain for both formulated and single crystal forms, although many mechanistic models have been proposed. Except in cases of strong shock, deformation consisting of yielding, plastic flow, and polymorphic phase transformations precedes initiation of detonation.^[32]

Constitutive equations describing the mechanics of materials are developed in a logical progression.^[33] This progression begins with understanding the structure of materials from point group to space group, including polymorphism, to defect structures, to deformation, beginning

with elasticity and progressing to a three-dimensional combined-stress theory of plasticity and including the first static yield conditions and post-yield behavior, before moving to dynamic yield conditions and post-yield behavior. We set out to follow this approach for explosives from structure to initiation and hydrodynamic behaviors, but we immediately found serious complexities with elasticity that limit accurate predictions beyond that state.

2 The Importance of Elasticity in Crystalline Explosives

Elasticity is critically important in our understanding and prediction of explosive materials, whether or not solid mechanics plays any role at all in initiation. Even if prompt shock in intentional initiation is strong, the structure and compressibility of the explosive are relevant. The importance in this case is outlined by the Zel'dovich, von Neumann, Doering (ZND) theory of detonation.^[8-10] The compressibility of the reactant, which is the bulk modulus and its derivative with pressure, with a Rayleigh line tangent to the compressibility of the detonation products, determines the peak hydrodynamic pressure upon detonation and the reaction zone of the decomposition.

There are many material responses in which it is important to understand non-initiating behaviors, including deformation and failure, since damage may alter the safety of the explosive material and sets a new initial condition for subsequent performance.

Finally, softer insults may induce unintentional initiation. These insults are typically associated with safety scenarios, and span many rates and mixed physical and chemical pathways. The degree to which each type of insult involves solid mechanics varies prior to reaching a hydrodynamic state, but all begin in this regime.^[34]

X-ray and neutron diffraction accurately determine crystal structures to high precision. Except in cases of high defect content or solid solutions, the starting structure of the material is usually well determined. Crystal structures are accurately determined for PETN, RDX, HMX, and TATB at standard temperature and pressure conditions.

The hydrodynamic link in the ZND model is perhaps most directly explored through compression experiments such as in the diamond anvil cell (DAC). DAC data for these materials and associated compressibility and phase behavior is an active area of research and so rich that it merits its own review. However, we can use a few examples to shed light on our focus on other methods for elastic property determination. Menikoff uses the example of HMX to demonstrate the importance of bulk modulus. Using all available published data on compressibility of HMX crystals, it is possible to fit an empirical compression curve through the data in so many ways that the extrapolation varies by more than 25% in compression at the detonation state, and this ambiguity is important in PBX materials containing HMX.^[13, 14] These data, with errors, from one DAC study and the compared fits are shown in Figure 1. Bulk moduli ranging from 16 to 24 GPa gave an excellent fit to this isothermal data. Fit ranges diverge even more when other data sets are included. The peak pressure can be accessed, at least for the Chapman-Jouget state, through inferential experiments that use metal expansion to fit equation of state (EOS) curves, but the approach from reactants is desirable to both validate the ZND theory and to add precision to the EOS. An accurate measurement of the full elastic tensor provides an anchor at points along the EOS, and this approach is especially useful if the full tensor determination can be made for other conditions, including temperature and pressure. Such measurements are possible, but they have been frustrated by large errors, and until recently these errors were not understood.

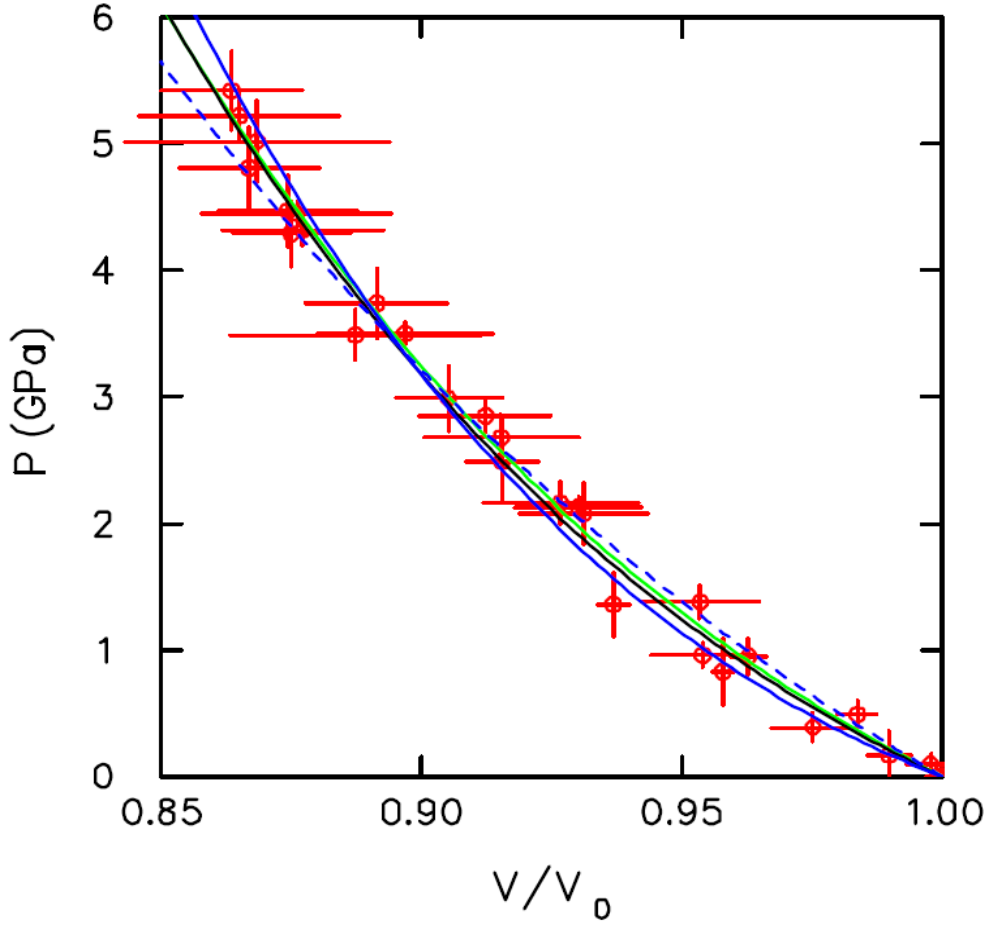


Fig. 1. Isothermal and shock Hugoniot data for HMX leads to large errors in extrapolation depending upon the fitting form and parameters of the EOS, as shown in the plot in the pressure-reduced volume plane with data from Gump and Peiris.^[35, 36] Bulk moduli ranging from 16 to 24 GPa yielded low-residual fits to this data set, which leads to extrapolations to pressures that vary by more than 25% at the detonation state. This error is further compounded when other data sets are included.^[12, 13]

Every ambiguity in the properties of materials from initial structure to the hydrodynamic state confounds attempts to develop models for mechanical behavior and possible chemical response. Beginning with molecular structure and motions, as determined through electronic and

vibrational spectroscopies, crystal structures are the first test of prediction. Because electronic structures, molecular vibrations, and crystal structures are typically so well characterized, a good starting point and validation is provided to predictions, even if crystal structure prediction itself is difficult given the soft, competitive intermolecular interactions. Prediction of small elastic perturbations of the crystal are themselves difficult as molecular and intermolecular interactions are subtle. Unfortunately, there is no way to be sure whether models that achieve known structures will accurately predict the perturbation response of these structures. If we had complete and accurate measurements of elastic response, in several physical conditions, elastic perturbation prediction would be physically bounded. Even the basic measurements have been prone to large errors and the origins of this error have not previously been understood. These errors in elasticity have serious consequences for predictive models when it is considered that every possible scenario we hope to predict – from defect structures to material deformation to phase changes to hydrodynamic flow and chemical reaction – begins with elastic deformation.

3 Measurement of Elasticity

Measurement of elastic constants by compression between platens is generally not possible for energetic materials because their anisotropic elasticity require too many geometries and because only relatively minute elastic strains are possible prior to brittle failure.^[37] Mechanical resonance techniques work well for these materials, provided that adequate samples can be made and that the crystals are of orthorhombic or higher symmetry. This symmetry requirement stems from the data analysis method by which the elastic tensor is determined from the resonances.^{[38-40][41]} Spanning orders of magnitude in frequency and volume, several techniques are available for the

determination of elastic tensors: resonant ultrasound spectroscopy (RUS),^[42] pulse-echo ultrasound (P-E), impulsive stimulated scattering (ISS),^[43] and Brillouin scattering.^[44]

All of these techniques have been used to measure elastic tensors for PETN and for RDX. For HMX, the monoclinic symmetry precludes unique solutions from data for the RUS technique, so there are fewer measurements. A comparison of measurements reveals large, non-systematic variations. With no obvious correlation to the material or measurement technique, differences had been ascribed to potential sample purity and processing variations.

P-E and ISS measurements of the tetragonal PETN-I elastic tensor compare well.^[40, 45] For orthorhombic α -RDX, P-E, two separate RUS measurements, and ISS compare well, while the first Brillouin scattering measurement yielded values significantly stiffer than the other measurements.^[40, 46-49] HMX, a more complicated crystal, showed even more disagreement in initial measurement, with differing results from complete and partial determinations by ISS, both disagreeing with a determination by Brillouin, which was, in contrast to the RDX difference, softer overall than the ISS results.^[39, 40, 50, 51] The ISS partial determination used only the quasi-longitudinal mode measured from one orientation of HMX, so the solution reported for the elastic tensor is not unique since the measurements substantially underdetermine the system. In fact, the quasi-longitudinal velocities from the partial ISS determination match well with the same ISS measurements from the full determination (*cf.* Fig. 2^[50]), which included all observed quasi-longitudinal and quasi-transverse modes for three distinct orientations of HMX. Since the ISS velocity data from the two studies is consistent and the measurements constrain the tensor much better in the second ISS study^[50], the elastic tensor from the second study should be used instead of the under-determined results of the first ISS measurements on HMX.^[51] The disparity in these elasticity determinations for RDX and for HMX has directed research for about the last

10 years towards understanding whether the variance is a consequence of the measurement technique or of sample variation, including purity, inherent or induced defects, or another physical mechanism.

The elastic tensor of PETN determined from Brillouin scattering and RUS measurements on the same crystalline sample showed variance in tensor components that persisted even when sample variation effects were removed, with anisotropic frequency dependence observed.^[52] The origin of this frequency dependence was not determined but initiated experiments to explore whether such dispersion might explain the differences in reported tensor components for RDX and HMX.

Photoacoustic measurements were performed in (100)-oriented RDX spanning acoustic frequencies from 0.5 to 15 GHz using ISS and picosecond acoustic interferometry (PAI).^[53] These measurements agreed with previous ultrasonic and ISS measurements at lower frequencies, but were contrary to Brillouin measurements. The possible reasons for contradiction with reported Brillouin results were unknown, but good agreement with other techniques and lack of acoustic dispersion over six orders of magnitude in frequency were evidence that there is no frequency-dependent relaxation process that couples to linear acoustic waves in RDX at acoustic frequencies up to 15 GHz. The anomalous Brillouin measurements for RDX, which used an excitation frequency higher than 15 GHz, still needed to be explained.

To resolve the contradiction in elasticity of RDX at high frequency and to investigate whether acoustic dispersion might be relevant above 15 GHz, the elastic tensor was recently determined again using Brillouin spectroscopy, with redundancy in velocity measurements, using multiple samples and with a detailed investigation of the data reduction technique.^[54] Brillouin measurements on five different RDX single crystals showed agreement with all previous

determinations *except* the original Brillouin report. Little variation was observed in the measured acoustic velocities in 5 different as-grown crystal samples, except for measurements that spanned regions of the crystals that were highly strained. Furthermore, the results showed that there is no frequency dispersion over many orders of magnitude when compared to all of the previous results, except, again, the previous Brillouin determination. The burden of demonstrating that the new results were correct was high, and required some explanation of the origin of inconsistencies in the previous data. The evaluation points to errors in the original report in velocity measurements and in their assigned modes, and to fitting procedures to produce tensor components from the measured velocities. There are multiple contradictions in the reported velocities for symmetrically equivalent phonons, and since contradictory velocities are reported for equivalent modes, the velocities themselves must be in error.^[55] Despite all of the interesting physical explanations that may have produced the reported discrepancies, it appears that the culprit in the end is an error in measurement and data reduction. It is worth spending some time discussing how these errors could arise, and prescribing both how to evaluate and prevent such errors in the future.

3.1 Evaluating Error in Measurements and Tensor Determinations

Most molecular crystals are low symmetry and anisotropic. A limited number of phonons are frequently measured and not all acoustic modes are observed for a given wave vector, either due to experimental limitations or, occasionally, because modes have the same frequency.

Observation of only a limited number of modes can result in subjective assignments of fast and slow transverse modes. Initial conditions of the analysis can substantially affect the resulting evaluation with a relatively small number of observed phonons. These effects often are not

incorporated into uncertainty analysis, so many elasticity measurements in explosives have reported unrealistically small uncertainties. This underestimation is due to reliance on the precision of the individual acoustic measurement rather than the stability of the overall tensor solution, including all aspects of the tensor refinement, and to a smaller extent, variations in material.

As there are fewer measurements for HMX and the monoclinic structure results in more complicated analysis, we will use available data to evaluate how errors in measurement or analysis might translate to errors in the full elastic tensor determinations. Full elastic tensors for HMX have been presented by one experimental measurement with Brillouin scattering^[39] and one full determination with ISS.^[50] Both determinations used acoustic velocity measurements to produce a tensor through numerical inversion of the Cristoffel determinant.

To investigate the possible sources of the discrepancies between the elasticity measurements of HMX, we analyzed the Brillouin data using all reported velocities for HMX associated with the Brillouin publication,^[39] listed comprehensively elsewhere.^[56] The analysis algorithm we employed utilizes a Levenberg-Marquardt algorithm to minimize errors between the measured acoustic velocities and those calculated from a trial elastic tensor. This algorithm was also used in the recent RDX Brillouin paper.^[54] Our error minimization routine did not find the same elastic tensor as reported,^[39] even if the elastic tensor reported was used as the initial conditions for the minimization routine. The elastic tensor components from the minimization also varied depending on the initial conditions from which the minimization was started. For monoclinic systems, the analytic solution for C_{22} can be calculated from the longitudinal velocity of the [010] phonon. The reported value for C_{22} (14.41 ± 0.06 GPa) in the publication^[39] does not

match the value calculated analytically from the velocity in the more comprehensive report (11.95 GPa).^[56]

In situations where the measurement velocities and directions and the low crystal symmetry give a complex potential energy surface for the minimization, local minima can be reached instead of the global minimum. Solution variation as a result of changing initial guess is a clear indication that the global minimum is not achieved. Large variations in solutions were observed in the comparisons we performed, suggesting that the solutions are highly unstable or that the minimization algorithm is inadequate. We suspect that the underlying cause of the instability is the availability of just 8 phonons with 14 unique modes in a system with so many degrees of freedom. This implies that the data is insufficient to uniquely determine the tensor.

To examine the effects of using a small number of phonons in determining the elastic tensor in a low symmetry crystal, we performed some demonstrative calculations using an over-determined data set on coesite, a metastable SiO₂ polymorph. Coesite is a monoclinic crystal like HMX and has a self-consistent, well-determined elastic tensor from acoustic velocities in 80 different crystallographic directions.^[57] We have used this complete data set for coesite, and the acoustic velocities of the Brillouin data for HMX^[56] to illustrate the difficulties that can arise from using a small number of phonons in the determination of a low symmetrythe elastic tensor. From the coesite data, we selected 8 phonons with 14 unique modes to be similar to the phonon directional distribution that was measured by Brillouin in HMX.^[b] We executed the Levenberg-Marquardt minimization routine on the full coesite dataset and on the dataset with the limited number of phonons. The starting parameters for the minimization routine were the coesite elastic tensor as reported. The results are shown in Table 1, along with Weidner and Carleton's

[b] Counting the first row listed in Weidner and Carleton, Table 1, as 1, the selected phonons were those from the following rows: 11, 13, 35, 42, 47, 59, 71, and 73.

originally reported tensor.^[c] We then employed Monte Carlo analysis to vary each of the velocities of the acoustic modes with a normal distribution with a full width at half maximum of 200 m/s, the estimated uncertainty as reported by Weidner and Carleton, and ran the minimization to yield the elastic tensors. Figure 2 shows the histogram results of the Monte Carlo analysis on the coesite data with all 80 measured phonons and on the coesite data from which we selected only 8 phonons. Despite using the same widths on the velocity distributions, the tensor components are significantly different, with uncertainties about an order of magnitude greater, on average, when the limited phonon dataset was used. Additionally, the distributions in uncertainties from the reduced phonon dataset do not correlate well with the elastic constants determined from the full dataset. The means and standard deviations from the Monte Carlo analysis for both the full and reduced datasets are given in Table 1. The large differences in the tensors and in their uncertainties that arise from reducing the number of phonons in the dataset illustrate the hazard of using a small data set to determine a low symmetry elastic tensor.

Table 1. Reduction of phonon direction and velocity data for monoclinic coesite. The first columns of data reproduce the published tensor parameters and uncertainties from Weidner and Carleton.^[57] The middle set of columns used the same full 80-phonon dataset but the minimization routine was a Levenberg-Marquardt minimization. The tensor was the result of a single minimization using the phonon directions and velocities as published. The Monte Carlo mean and Monte Carlo standard deviation show the mean and standard deviation of 10^4 trials of the Monte Carlo calculations, which used the phonon directions as published but varied the

[c] Weidner and Carleton used an analysis method different from the one we employed, and they determined the uncertainty limits based on his algorithm that included the effects of the spatial distribution of the measured phonons and the stability of the tensor solution to the initial parameters.

velocities in a normal distribution with a width of 200 m/s centered on the published velocities.

The final set of columns shows the same parameters as the middle set, but it is the result of using only the selected 8-phonons as explained in the text. This last dataset reveals large changes to the tensor elements and to their uncertainties. Histograms of the Monte Carlo results from the middle and final sets of columns are shown in Fig. 2.

	Coesite results as published		Full coesite measurements with Levenberg-Marquardt minimization and Monte Carlo uncertainty analysis			Limited number of coesite measurements with number and directions of phonons similar to HMX Brillouin measurements		
	Tensor	uncertainty	Tensor	Monte Carlo mean	Monte Carlo std dev	Tensor	Monte Carlo mean	Monte Carlo std dev
C ₁₁	160.8	2.9	160.3	160.2	2.9	130.2	132.2	38.4
C ₁₂	82.1	4.2	81.2	80.6	4.4	53.6	59.0	28.2
C ₁₃	102.9	6.6	103.1	103.3	6.3	105.3	101.9	30.8
C ₁₅	-36.2	1.8	-35.9	-35.9	1.8	-27.5	-35.3	19.1
C ₂₂	230.4	2.6	229.4	229.4	2.5	233.8	233.0	7.8
C ₂₃	35.6	8.1	35.7	35.8	7.4	68.5	59.3	18.5
C ₂₅	2.6	4.0	3.8	3.7	3.8	16.5	12.4	21.9
C ₃₃	231.6	4.4	230.4	230.4	4.4	224.0	220.6	13.0
C ₃₅	-39.3	2.4	-39.5	-39.4	2.4	-31.1	-34.7	17.3
C ₄₄	67.8	3.0	67.8	67.5	3.2	53.1	56.0	7.1
C ₄₆	9.9	2.0	9.6	9.5	2.0	11.8	12.1	4.2
C ₅₅	73.3	2.3	73.0	72.9	2.4	98.3	97.6	22.2
C ₆₆	58.8	1.8	58.2	58.5	2.0	56.7	57.2	4.4

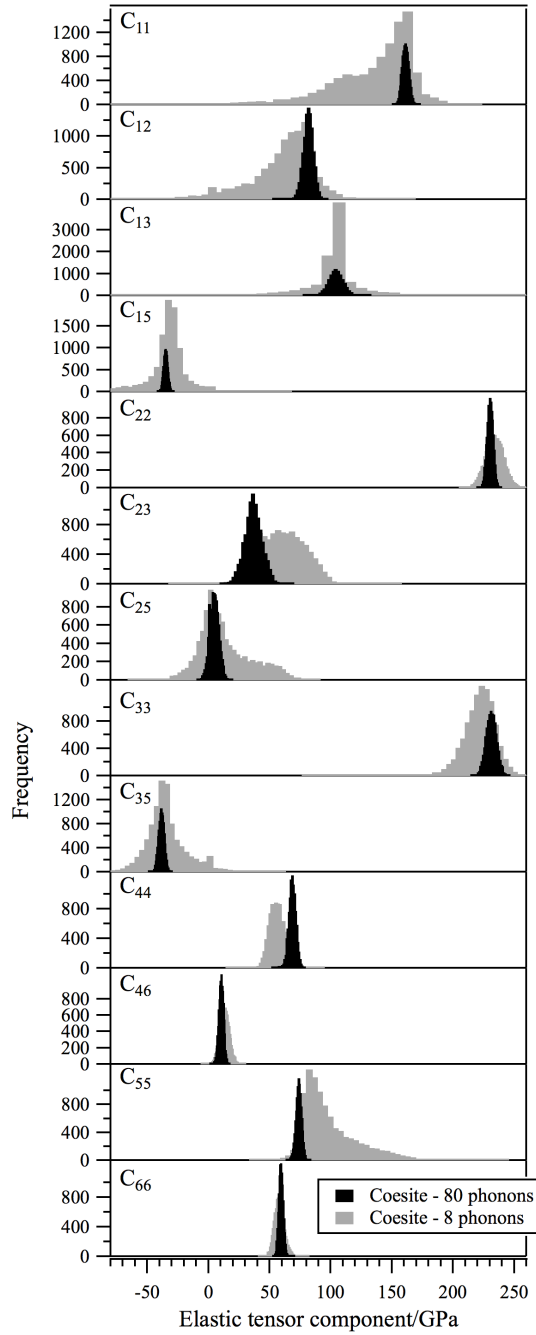


Fig. 2. Histograms of the Monte Carlo distributions of the elastic tensor components for coesite using Weidner and Carleton's full dataset^[57] and the reduced dataset with 8 phonons. Normal distributions of the velocities with widths of 200 m/s were used in the Monte Carlo evaluation.

To demonstrate the effect of the coesite example on the available HMX data, Fig. 3 shows the same type of Monte Carlo analysis with 10^4 trials in which the acoustic data from Stevens and Eckhardt^[56] was evaluated with 1% uncertainties in the velocity measurements. The shapes of the distributions in Fig. 3 are more normal than those in the 8 phonon dataset of Fig. 2, but their accuracy cannot be determined since there is not a heavily overdetermined dataset with which to compare and the shapes of the distributions do not necessarily imply that the result is accurate (consider, for example, C_{44} in Fig. 2).

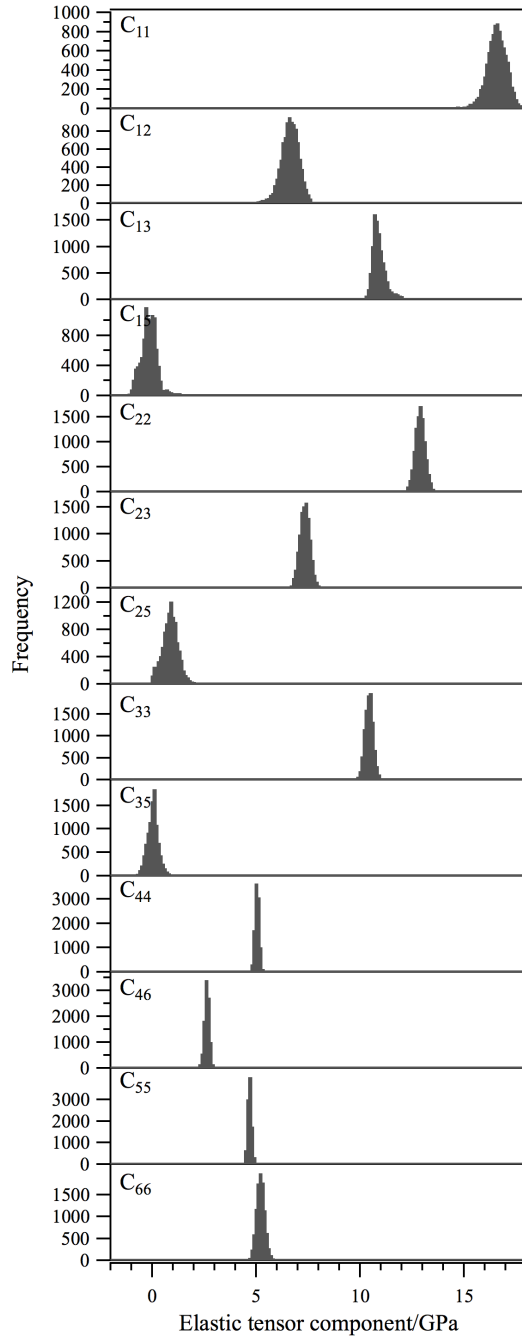


Fig. 3. Histograms of the Monte Carlo distributions of the elastic tensor of HMX using the velocities and directions associated with the Brillouin determination^[56] and a normal velocity distribution of 1%.

An often-overlooked source of additional error is the stability of the numerical solution. The initial conditions for the error minimization can have a substantial influence on the final solution if the number and directions in which the measurements are made result in a complex landscape for the multivariable minimization. When minimizing errors with large numbers of variables, such as 13 tensor components for monoclinic crystals, local minima may be common. Therefore, the stability of the numerical minimization to variations in the starting parameters must be evaluated. Monte Carlo evaluation of the minimization of the Cristoffel determinant illustrates numerically how local minima, arising from limited directional acoustic data, may cause error in determining tensor elements in low-symmetry systems. In this approach, the minimization is repeated many times, allowing for the initial guess to vary. The sensitivity of the resulting tensor to the initial guess can be viewed as a histogram, which shows the statistical likelihood of multiple minima and the overall error that these minima introduce. To represent the large uncertainties indicative of an initial guess used for materials with an undetermined elastic tensor, we set the initial parameters to be randomly distributed about Weidner and Carleton's coesite tensor with the widths of the distributions as ± 75 GPa for C_{11} , C_{22} , and C_{33} and as ± 50 GPa for all other components.^d The histograms of the Monte Carlo results are shown in Fig. 4. Using the full 80 phonon coesite dataset, the vast majority of the solutions found converged to the coesite tensor reported. Conversely, when using the 8-phonon dataset, the changes in the initial parameters of the minimization frequently resulted in different elastic tensor results.

[d] Due to the large widths of the distributions for the initial guesses, the randomly generated initial guesses sometimes resulted in a physically unrealistic tensor, *i.e.* when the tensor was used to calculate the acoustic velocities for the relevant phonons, imaginary velocities were calculated. The trials for which the initial guesses created physically unrealistic tensors resulted in non-convergence of the minimization routine and were excluded from the histograms shown in Fig. 4. For the 10^3 trials calculated, 177 of the 80 phonon trials and 100 of the 8 phonon trials resulted in this non-convergent condition.

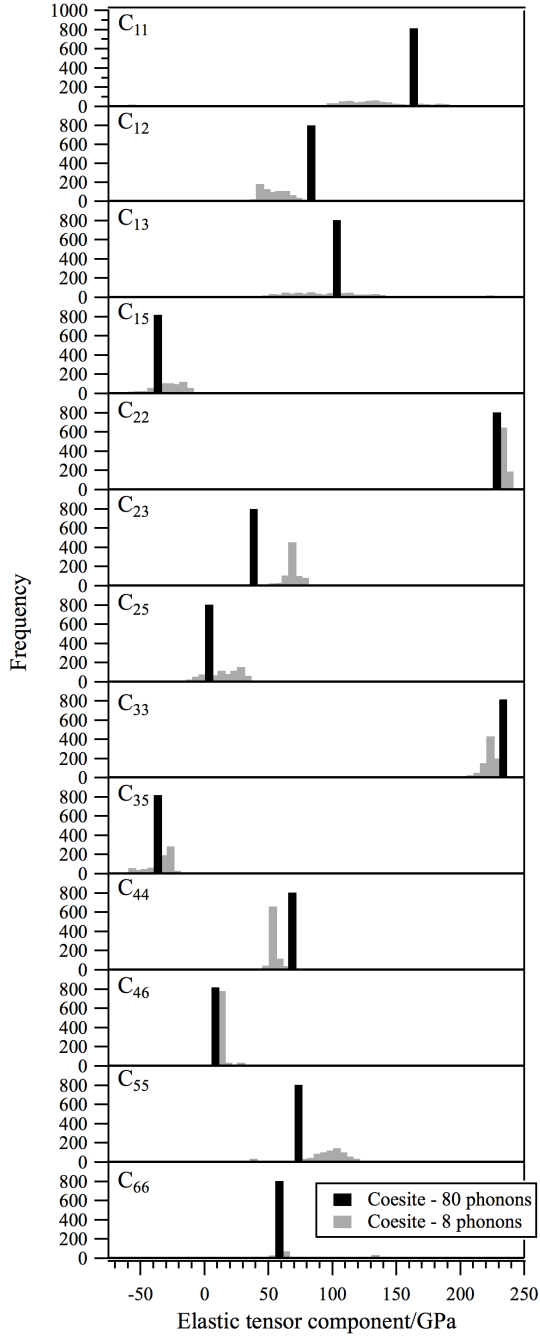


Fig. 4. Histograms of the Monte Carlo distributions of the elastic tensor components of coesite that employed variations in the initial parameters of the multivariable minimization routine. The black histograms show the results for the dataset of all 80 phonons measured by Weidner and Carleton.^[57] These data result in a single, stable solution for the elastic tensor. The

grey histograms used the dataset of only 8 phonons, and they show that there are many local minima in the multivariable minimization that can produce incorrect tensor results.

We repeated this same Monte Carlo evaluation on the initial parameters for the Brillouin HMX data with distributions of ± 7.5 GPa for C_{11} , C_{22} , and C_{33} and of ± 5 GPa for all other components with the distributions centered on the tensor reported by Stevens and Eckhardt.^[39] These results are shown in Fig. 5. The large distributions in many of the tensor parameters indicate that the minimization surface is highly complex and that changing the initial parameters of the minimization can significantly influence the tensor result.

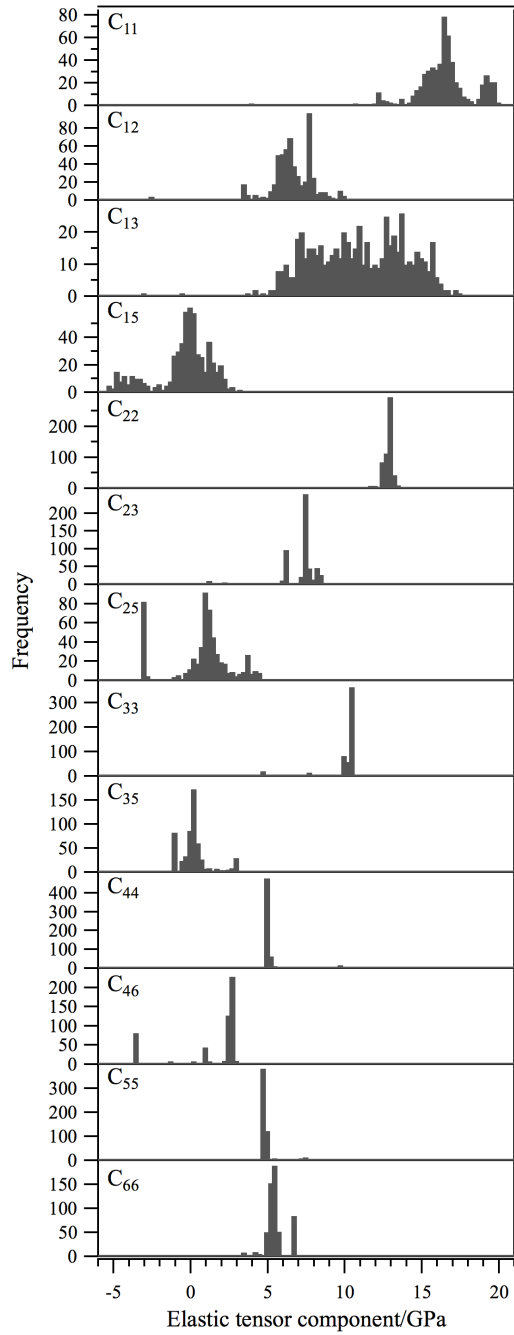


Fig. 5. Histograms of the Monte Carlo distributions of the elastic tensor components of HMX using variations in the initial parameters of the multivariable minimization routine using only 8 phonons. These distributions show multiple local minima and large uncertainties.

Determining elastic tensors in these crystals requires a high degree of redundancy of measurements of acoustic velocities, on multiple samples, and a statistical evaluation of the reduction of the velocities to the tensor components. Due to the complexity of elasticity in low symmetry materials and the occasionally subjective assignment of acoustic modes, all acoustic velocity measurements and pertinent geometries be made available when data are published to permit evaluation of the data reduction and consistency in detail. Such evaluation is critical if the values are to be used in simulations of material response.

4 Prediction of Elastic Tensors

While predictions of structure are easily checked against structure determinations that are known to be of high accuracy, until now, the elastic tensor measurements were not significantly constraining to compare to deformation predictions, nor were true errors known for the measurements. Prediction tools for elasticity are important because (1) not all energetic molecular crystals are readily available as pristine single crystals, so measurements may not be possible by the available techniques, (2) crystalline phases accessed under high pressure may not be recoverable to standard temperature and pressure conditions, and (3) even if they are, we have shown that the complete tensor determination requires a significant amount of work to have high confidence in the results. Hence, capabilities for accurate computation and prediction of the tensor of single crystal elastic constants are appealing goals.

4.1 Computational Approaches

An interatomic potential gives the potential energy of the system as a function of the relative positions of all of the atoms.^[58, 59] Single crystal elastic constants have been computed using

interatomic potentials since at least the mid-1950s.^[60] The most common route to the computation of elastic constants involves the direct evaluation of the elastic strain energy, $W(\epsilon)$, upon the distortion of the crystal by the application of an Eulerian strain tensor, ϵ_{ij} , where in Voigt notation,

$$\begin{pmatrix} \epsilon_1 & \epsilon_6 & \epsilon_5 \\ \epsilon_6 & \epsilon_2 & \epsilon_4 \\ \epsilon_5 & \epsilon_4 & \epsilon_3 \end{pmatrix} = \begin{pmatrix} \epsilon_{11} & 2\epsilon_{12} & 2\epsilon_{13} \\ 2\epsilon_{12} & \epsilon_{22} & 2\epsilon_{23} \\ 2\epsilon_{13} & 2\epsilon_{23} & \epsilon_{33} \end{pmatrix} \quad (1)$$

and

$$W(\epsilon) = V_0 \left[\sum_i \sigma_i \epsilon_i \xi_i + \frac{1}{2} \sum_{i,j} C_{ij} \epsilon_i \xi_i \epsilon_j \xi_j \right], \quad (2)$$

where V_0 is the unstrained volume of the simulation cell, σ_i is an element of the stress tensor (in Voigt notation), $\xi_i = 1$ if $i \leq 3$ or 2 if $i \geq 4$, and C_{ij} is the matrix of single crystal elastic constants.^[61-63] The strain energy is computed over a small set of strains of magnitude typically less than 1%, and a least square fit is made to the resulting parabola with a polynomial to obtain the elastic constant or linear combination of elastic constants probed by the applied strain. The use of small strains in the calculation is necessary to ensure that i) the Eulerian and Lagrangian strain measures are essentially indistinguishable and ii) the applied strain does not exceed the ideal strength of the solid.^[64] The latter is particularly important in complex molecular crystals with many internal degrees of freedom.

An alternative route to the computation of single crystal elastic constants employs the stress tensor derived from the interatomic potential either numerically or via the virial theorem,^[58] where the dependence of the computed stress on the applied strain yields the elastic constants directly via the generalized form of Hooke's law,

$$C_{ij} = \frac{\partial \sigma_i}{\partial \varepsilon_j} \quad (3)$$

The strain energy or direct approaches to the computation of elastic constants are relatively straightforward to implement and apply. However, the calculations should be performed starting from a simulation cell where the stress tensor and all interatomic forces are fully relaxed. The internal degrees of freedom of the simulation cell should also be relaxed again to a high tolerance upon each distortion of the lattice. These procedures are computationally demanding for low-symmetry molecular crystals.

The strain energy approach, Eq. 2, is of practical use only at zero temperature. The direct method, Eq. 3, can instead be used in molecular dynamics simulations in the canonical ensemble (constant number of particles, volume, and temperature, NVT) to generate single crystal elastic constants as a function of temperature.^[65] At finite temperature the stress tensor used to derive the elastic constants includes contributions from both the interatomic forces and momenta. The use of the direct method within a molecular dynamics framework is computationally demanding since it requires i) a long-duration simulation in the isothermal-isobaric (NPT) ensemble to determine with high fidelity an equilibrium set of lattice parameters at the target temperature and pressure, and ii) at least 3 to 9 long duration simulations in the canonical ensemble during which the ensemble average of the stress tensor is computed for each distortion, ε_j . For an orthorhombic molecular crystal, for instance, this translates to 19 to 55 simulations each comprising of the order 10^6 time steps to evaluate the 9 independent elastic constants at each temperature and pressure.

The Parrinello-Rahman boundary condition^[66-68] provides a more elegant route to the computation of the temperature dependence of single crystal elastic constants. The equations of motion for the Parrinello-Rahman boundary condition are derived from an extended Lagrangian that includes a strain energy arising from the distortion of the simulation cell. The application of the Parrinello-Rahman boundary condition gives rise to fluctuations in the dimensions and shape of the simulation cell that are consistent with the isothermal-isostress ensemble, $N\sigma T$. The fluctuations in the dimensions of the simulation cell are related to the elastic compliance tensor, s_{ijkl} , at the specified σ and temperature,

$$s_{ijkl} = \frac{k_B T}{V_0} \langle \eta_{ij} \eta_{kl} \rangle, \quad (4)$$

where k_B is Boltzmann's constant, η_{ij} are elements of the Lagrangian strain tensor, and $\langle \rangle$ denotes an ensemble average.^[67] The matrix of single crystal elastic constants, C_{ij} , are derived from the compliance tensor by first transforming it into a 6×6 matrix in Voigt notation via the rules,

$$S_{mn} = \begin{cases} s_{ijkl} & \text{if } m \text{ and } n \leq 3 \\ 2s_{ijkl} & \text{if } m \text{ or } n > 3 \\ 4s_{ijkl} & \text{if } m \text{ and } n > 3 \end{cases} \quad (5)$$

followed by the computation of its matrix inverse, that is, $C = S^{-1}$.^[69, 70] While the Parrinello-Rahman boundary condition will in principle yield all of the single crystal elastic constants of a molecular crystal from one 10^6 - 10^7 time step trajectory, its application is often fraught with difficulties.^[71] The results obtained from trajectories computed using the Parrinello-Rahman boundary conditions tend to depend sensitively on the properties of the barostat used to achieve the target stress. As a result, the Parrinello-Rahman method is typically employed within a

Monte Carlo simulation framework that avoids the application of a barostat completely.^[71]

Nevertheless, we report a set of elastic constants for RDX obtained from a molecular dynamics trajectory computed using the Parrinello-Rahman framework that is of comparable accuracy to those obtained using the direct method but is a fraction of the total computational cost.

4.2 Application to α -RDX

We have computed the elastic constants of α -RDX at zero and finite temperatures using the four methods discussed in the previous section. The calculations at zero temperature employed dispersion-corrected density function theory with the strain energy (Eq. 2) and direct (Eq. 3) approaches. The calculations at finite temperature were performed using the Smith-Bharadwaj force field for nitramines^[72] via the direct (Eq. 3) and Parrinello-Rahman (Eqs. 4-5) approaches. The elastic constants of RDX have been evaluated experimentally and computationally using a number of approaches such that the accuracy of our predictions can be assessed.

4.2.1 Dispersion-Corrected Density Functional Theory at Zero Temperature

Density functional theory is considered to be the standard in terms of accuracy for modeling interatomic bonding in condensed phase systems.^[73, 74] Traditional implementations of density functional theory tend to underestimate the strength of weak dispersion, or van der Waals interactions, between molecules.^[75] Since weak dispersion interactions contribute significantly to cohesion in organic molecular crystals, traditional density functional theory systematically underestimates equilibrium mass densities. Dispersion-corrected density functional theory aims to improve the description of dispersion interactions either through an improved model of the underlying electronic structure, or via the addition of a set of atom-centered pair potentials.^[76-85]

We have taken the latter route and apply in our calculations the 3rd generation empirical dispersion corrections (DFT-D3(BJ)) of Grimme and co-workers.^[79]

Our dispersion-corrected density functional theory calculations were performed using the Quickstep package with the cp2k code^[86] with the generalized gradient approximation exchange-correlation functional of Perdew, Burke, and Ernzerhof (PBE).^[87] The TZV2P Gaussian basis set^[86] with Goedecker-Teter-Hutter pseudopotentials^[88] was used in conjunction with energy cutoffs for the dual plane wave basis of 1000 Ry and REL_CUTOFF = 80 Ry. The TZV2P basis gave a predicted equilibrium volume for the RDX unit cell that changed only at the fourth significant figure upon increasing the basis set size to QZV2P and QZV3P and as a result we believe this basis to be optimal for modeling RDX.

The α -RDX unit cell was optimized by static relaxation using the structure determined by Choi and Prince^[89] as a starting configuration. The self-consistent field calculations were performed to a tolerance of 10^{-7} and the relaxation of the atomic coordinates was terminated when the magnitude of the force acting on every atom was less than 5×10^{-6} eV/Å. The final lattice parameters were $a = 13.383$, $b = 11.552$, and $c = 10.857$ Å with $V_0 = 1678.553$ Å³. These values compare very well to those obtained by Taylor at a similar level of theory,^[90] as well as experiment.

The single crystal elastic constants C_{11} , C_{22} , and C_{33} were computed by the application of non-volume conserving strains of the form,

$$\varepsilon = \begin{pmatrix} 1+\delta & 0 & 0 \\ 0 & 1 & 0 \\ 0 & 0 & 1 \end{pmatrix}, \quad (6)$$

$$\varepsilon = \begin{pmatrix} 1 & 0 & 0 \\ 0 & 1+\delta & 0 \\ 0 & 0 & 1 \end{pmatrix}, \quad (7)$$

and,

$$\varepsilon = \begin{pmatrix} 1 & 0 & 0 \\ 0 & 1 & 0 \\ 0 & 0 & 1+\delta \end{pmatrix}, \quad (8)$$

respectively, where $-0.0025 \leq \delta \leq 0.0025$ in increments of $\delta = 0.0005$. These strain tensors also allowed us to evaluate C_{12} , C_{13} , and C_{23} by the direct approach, since, for example, $C_{12} = \partial\sigma_1/\partial\varepsilon_2$. The remaining elastic constants were computed via the application of the volume conserving strain tensors listed in Ref. [63]. The internal degrees of freedom in the RDX simulation cell were relaxed after the application of the strain tensors until the magnitude of the force acting on every atom was less than 5×10^{-5} eV/Å before the evaluation of the total potential energy and stress tensor.

We present in Table 2 the single crystal elastic constants of RDX at zero temperature evaluated using the strain energy and direct approaches via dispersion corrected density functional theory (DFT-D3(BJ)). The elastic constants computed by Taylor using at the DFT-D3 level of theory with the PBE exchange-correlation functional and the QZV2P or QZV3P Gaussian basis sets via the direct approach are also presented as a comparison with our results.^[90] We provide two values for C_{12} , C_{13} , and C_{23} since each elastic constant can be computed by the application of two different strain tensors, that is, $\partial\sigma_1/\partial\varepsilon_2 = \partial\sigma_2/\partial\varepsilon_1$, for example. We also present for each set of elastic constants their root-mean-square (RMS) error with respect to the elastic constants measured by Bolme and Ramos at room temperature.^[54]

Table 2. The single crystal elastic constants of α -RDX in GPa computed at zero temperature using DFT-D3(BJ) by the strain energy (Eq 2) and direct (Eq 3) approaches. Similar calculations by Taylor from Ref^[90] are also presented. The root mean square error between the sets of computed elastic constants and the experimental values of Bolme and Ramos measure the level of agreement between the calculations and experiment.

Tensor component	Strain energy (GPa)	Direct (GPa)	Taylor (direct) (GPa)
C_{11}	25.9	25.7	29.958
C_{22}	20.6	20.8	25.508
C_{33}	22.2	21.9	23.610
C_{44}	6.15	5.86	5.343
C_{55}	4.51	4.62	4.829
C_{66}	7.30	7.29	8.586
C_{12}	8.08	7.74 & 7.74	7.484
C_{13}	4.84	4.42 & 4.45	4.523
C_{23}	7.21	7.02 & 7.07	5.282
RMS error	1.296	1.274	2.915

The elastic constants computed by the strain energy and direct methods as part of this work are mutually consistent as expected. Nevertheless, individual elastic constants may differ by ± 0.2 GPa depending on the method of calculation. The two values for each of C_{12} , C_{13} , and C_{23} obtained by the direct approach each differ by less than 1%. The agreement between the two calculations for each of C_{12} , C_{13} , and C_{23} from the direct method as well as the agreement between the direct and strain energy approaches provides a consistency-check for the calculations that is useful for identifying errors. The RMS error for both sets of computed results with respect to the experimental data from Bolme and Ramos^[54] are almost identical and are less than 1.3 GPa. The zero temperature, zero pressure elastic constants presented by Taylor are generally in good agreement with our data. However, the RMS error between Taylor's elastic constants and experiment of 2.9 GPa is higher than those from our calculations. This discrepancy can be attributed to our use of different basis sets, dispersion corrections, and tolerances on the relaxation of the internal degrees of freedom.

The elastic anisotropy of an orthorhombic crystal can be quantified by the shear anisotropy factors

$$A_1 = \frac{4C_{44}}{C_{11} + C_{33} - 2C_{13}}, \quad (9)$$

$$A_2 = \frac{4C_{55}}{C_{22} + C_{33} - 2C_{23}}, \quad (10)$$

and,

$$A_3 = \frac{4C_{66}}{C_{11} + C_{22} - 2C_{12}}. \quad (11)$$

Each factor equals unity for an elastically isotropic material.^[63] Any departure of the values from unity is a measure of the degree of shear anisotropy. The values of A_1 , A_2 , and A_3 derived from

our computed elastic constants, data from Ref^[90], and experiment are presented in Table 3. The anisotropy factors derived from experimental data reveal that A_1 and A_2 indicate large elastic anisotropy while A_3 corresponds to a high level of elastic isotropy. All three sets of calculated elastic constants capture the relative values of A_1 , A_2 , and A_3 well. However, better quantitative agreement with experiment is obtained from the DFT-D3(BJ) calculations with the TZV2P basis set reported here.

Table 3. Shear anisotropy factors for RDX computed from the elastic tensors derived from the elastic tensors obtained from the strain energy and direct approaches, Ref. [90], and the room temperature experimental data from Bolme and Ramos.^[54]

	Strain energy	Direct	Taylor ^[90]	Experiment ^[54]
A_1	0.640	0.605	0.480	0.665
A_2	0.636	0.645	0.501	0.641
A_3	0.951	0.940	0.848	1.025

Based on the sets of single crystal elastic constants for α -RDX reported here and in Ref. [90] that are derived from dispersion-corrected density functional theory calculations, it is clear that computational methods are capable of providing quantitatively accurate predictions for the elastic properties of energetic molecular crystals. However, the results are evidently sensitive to the details of the calculation, such as the basis set or plane wave cut-off energy, and the precise form of the dispersion corrections. Furthermore, electronic structure calculations at zero temperature do not take into account anisotropic, temperature-dependent softening of the moduli.

4.2.2 Elastic Constants at Finite Temperature via Molecular Dynamics Simulations

First principles electronic structure calculations based on density functional theory are far too computationally expensive to be applied in long-duration molecular dynamics simulations on the thousands of atoms that are required to compute elastic constants at finite temperature. The non-reactive force field for nitramines developed by Smith and Bharadwaj^[91, 92] is computationally very efficient and it has been demonstrated to capture the structure of the α -RDX unit cell, the α -to- γ phase transformation, and the properties of crystal defects in RDX with at least qualitative

accuracy.^[24, 29, 65, 92-94] The Smith-Bharadwaj force field remains a popular tool for the study of RDX under a range of stimuli.

We have computed the elastic constants of RDX at 300 K and zero pressure using the direct method (Eq. 3) and the Parrinello-Rahman boundary condition with the Bharadwaj force field as implemented in the LAMMPS package.^[95] Our simulations used simulation cell comprising $3 \times 3 \times 3$ α -RDX unit cells under three dimensional periodic boundary conditions and a time step of the integration of the equations of motion of 0.5 fs. The use of larger simulation cells did not affect the computed elastic constants. The ensemble average of the lattice parameters of the α -RDX unit cell at 300 K and zero pressure from isothermal-isobaric (NPT) molecular dynamics trajectories are $a = 13.496$, $b = 11.554$, and $c = 10.560$ Å, with $V_0 = 1646.650$ Å³. All three lattice parameters are in excellent agreement with experiment and our DFT-D3(BJ) calculations.

The elastic constants derived from isothermal-isostress ($N\sigma T$) simulations using the Parrinello-Rahman formalism were found to be sensitive to the properties of the barostat implemented in LAMMPS. Consistency between the elastic constants obtained from the direct method and the Parrinello-Rahman formalism could be obtained only if the thermostat chains on the barostat were removed.^[96] Finally, the time constant over which the barostat relaxes the stresses was found to yield sensible elastic constants when set in the range 1000 to 2000 fs. These time intervals are consistent with the heuristic argument that pressure fluctuations should be relaxed over the time interval required for an acoustic phonon to traverse the simulation cell. Measured sound velocities in RDX are of the order 3500 m/s,^[53] yielding a time constant of approximately 1200 fs for our simulation cell.

The nine independent elastic constants of α -RDX computed via the Parrinello-Rahman formalism are presented as function of the simulation time in Fig 6. It is evident that trajectories approaching 4×10^6 time steps are required to converge the values of the elastic constants to within about 1 GPa. The converged values are presented in Table 4.

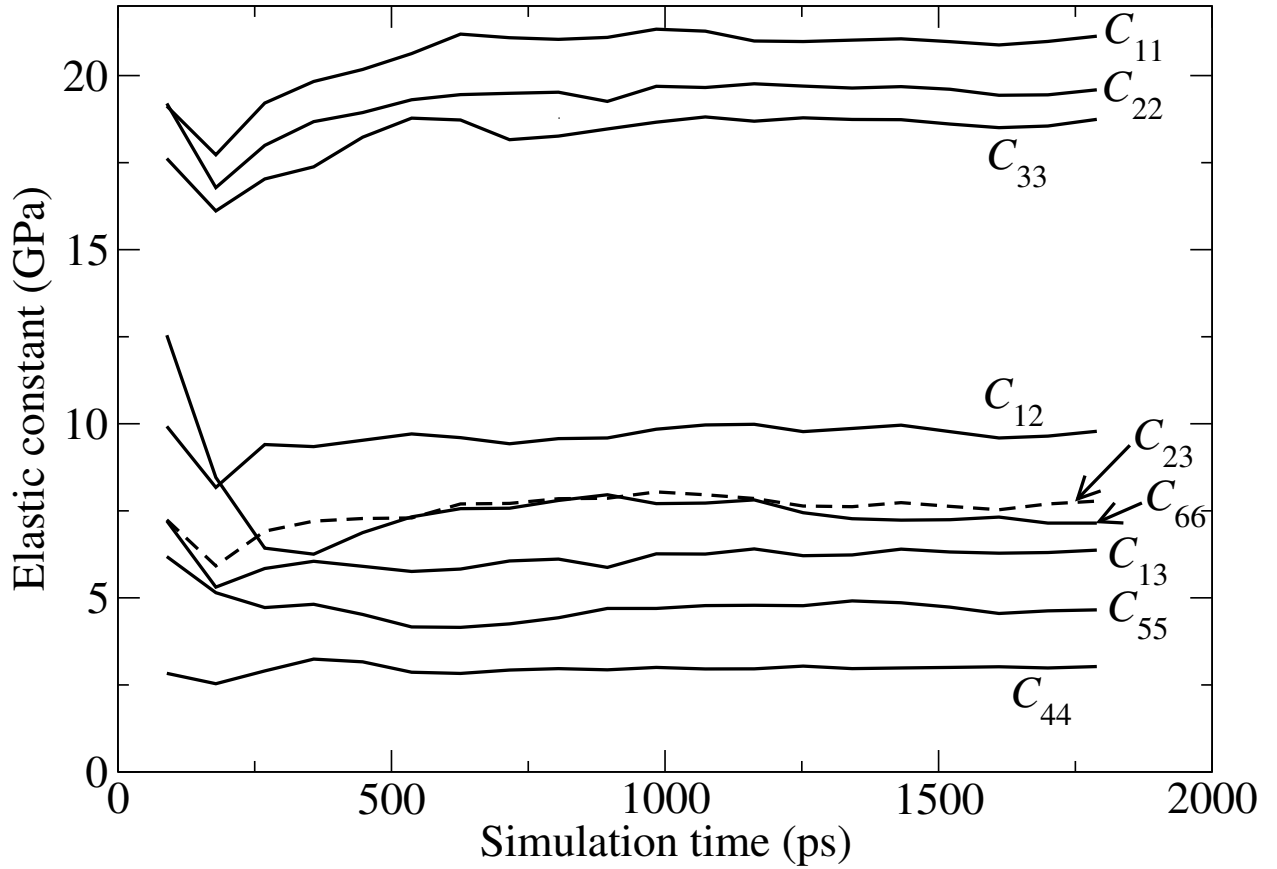


Figure 6. Single crystal elastic constants of α -RDX computed at 300 K via the Parrinello-Rahman method as function of the length of ensemble average of the strain fluctuations.

Whereas in this case the elastic constants appear to reach steady values after averaging the strain fluctuations over only 1 ns, depending on the temperature, pressure, or the properties of the barostat, significantly longer trajectories may be required.

Table 4. Single crystal elastic constants of α -RDX in GPa at room temperature and zero pressure computed using the Smith-Bharadwaj force field (this work and Munday *et al.*^[65]), and the Sorescu-Rice-Thompson potential energy surface for RDX.^[97] The elastic tensor measured by Bolme and Ramos^[54] at room temperature by Brillouin spectroscopy is presented for comparison.

Elastic constant	Parrinello-Rahman (this work)	Direct (this work)	Direct ^[65]	Parrinello-Rahman with Monte Carlo sampling ^[97]	Experiment ^[54]
C_{11}	21.1	22.1	25.0	26.9	25.8
C_{22}	19.6	20.4	23.8	24.1	20.1
C_{33}	18.7	19.9	23.4	17.7	18.9
C_{44}	3.03	2.92	3.1	8.4	5.3
C_{55}	4.66	4.85	7.7	5.3	4.2
C_{66}	7.15	7.26	5.2	7.6	7.2
C_{12}	9.78	9.56 & 9.61	10.6	6.27	8.3
C_{13}	6.37	5.96 & 5.82	7.6	5.68	6.4
C_{23}	7.78	7.52 & 7.74	8.80	6.32	6.4

The accuracy of the elastic constants obtained from our $N\sigma T$ molecular dynamics simulations was assessed by applying the direct method (Eq. 3) at finite temperature. The same $3 \times 3 \times 3$ unit cell with equilibrated lattice parameters was used the starting configuration for a series of simulations in the canonical ensemble. The simulation cell was deformed by applying the strain tensors given in Eqs. 6-8 with $-0.004 \leq \delta \leq 0.004$ in increments of $\delta = 0.001$. A larger strain increment than in our density functional theory calculations was used owing to the statistical noise in the long ensemble averages of the elements of the stress tensor. Each trajectory was allowed to thermally equilibrate for 50 ps after which we computed ensemble averages of the elements of the stress tensor over at least 4.5×10^6 time steps, or 2.25 ns. The resulting set of elastic constants is presented in Table 4.

The two sets of elastic constants that we derived from the Smith-Bharadwaj force field using the Parrinello-Rahman and direct approaches are in good qualitative agreement with, but systematically softer than those tabulated by Munday *et al.* Furthermore, both sets of elastic constants computed here, as well as those computed by Sewell and Bennett give $C_{66} > C_{55}$ whereas those tabulated by Munday *et al.* indicate that $C_{66} < C_{55}$. We attribute these discrepancies to the use in Ref^[65] of smaller simulation cell, a larger range of strains, and shorter ensemble averages. A positive conclusion from this work is that the application of the Parrinello-Rahman method in a molecular dynamics framework yields a set single crystal elastic constants that are in excellent quantitative agreement with those obtained from the direct approach but at a significantly smaller computational cost.

We also list in Table 4 the set of elastic constants of α -RDX computed by Sewell and Bennett^[97] using the potential energy surface for nitramines developed by Sorescu, Rice, and

Thompson^[98-101] with rigid molecules. Sewell and Bennett sampled the strain fluctuations required by the Parrinello-Rahman method (Eq. 4) using Monte Carlo methods. While the Sorescu-Rice-Thompson potential energy surface evidently predicts elastic constants that are stiffer than those derived from the Smith-Bharadwaj force field, they are in good quantitative agreement with the available experimental data.

4.3 Computed Elastic Constants for Other Energetic Molecular Crystals

4.3.1 TATB

Planar TATB molecules form a layered triclinic unit cell that features strong intermolecular hydrogen bonding. The low-symmetry triclinic unit cell gives rise to 21 independent elastic constants. All 21 elastic constants were computed by Bedrov *et al.*^[102] using non-reactive polarizable and non-polarizable force fields that were developed by the authors. Bedrov *et al.* computed single crystal elastic constants via fluctuations in the Lagrangian strain tensor (Eq. 4). However, these simulations combined molecular dynamics trajectories in the canonical ensemble with Monte Carlo sampling of variations in the shape of the simulation cell. The set of elastic constants computed at 300 K and atmospheric pressure that are tabulated in Ref. [102] are presented in Table 5. Using the same Parrinello-Rahman approach the authors also computed the dependencies of the single crystal elastic constants on temperature and pressure.

Valenzano *et al.*^[103] reported first principles electronic structure calculations of a subset of the elastic constants of TATB. These authors used a large Gaussian basis set, 6-311G(d,p) with a dispersion-corrected version of the B3LYP hybrid exchange-correlation functional and computed elastic constants via evaluating the strain energy, Eq. 2. As we demonstrated for α -RDX in Section 4.2.1, this methodology yields single crystal elastic constants that can be in

excellent agreement with experiment. Valenzano *et al.* went further by attempting to capture the temperature dependence of the elastic constants by performing their zero temperature calculations on a simulation cell that is constrained to the measured mass density at a given temperature. Those elastic constants reported by Valenzano *et al.* are presented in Table 5.

The pressure dependence of a sub-set of the elastic constants of TATB were computed by Ojeda and Cagin at zero temperature using a generic, non-reactive force field.^[104] All eight of the elastic constants reported in Ref. [104] were found to change discontinuously upon a pressure-induced transformation in the hydrogen bonding network of the crystal that was deduced from a series of condensed-phase density functional theory calculations. Repeating these elastic constant calculations with the Bedrov force field for TATB^[102] and/or dispersion-corrected density functional theory would be valuable. Predicted elastic constants have been used to develop thermoelastic constitutive relations for TATB.^[105]

Table 5. Computed elastic constants of TATB at 300 K from Refs. ^[102] and ^[103].

	Bedrov <i>et al.</i> (non- polarizable force field)	Bedrov <i>et al.</i> (polarizable force field)	Valenzano <i>et al.</i> (DFT-D)
C_{11}	57.7 ± 0.5	65.7 ± 0.5	78.4
C_{22}	58.0 ± 1.0	62.0 ± 1.0	-
C_{33}	17.0 ± 0.5	18.3 ± 0.5	19.7
C_{44}	1.0 ± 0.3	1.4 ± 0.3	0.9
C_{55}	0.6 ± 0.2	0.68 ± 0.06	-
C_{66}	20.3 ± 0.8	21.6 ± 0.7	29.7
C_{12}	16.2 ± 0.7	18.5 ± 0.5	16.8
C_{13}	3.2 ± 0.5	4.0 ± 2.0	0.8
C_{14}	0.1 ± 0.1	-0.2 ± 0.3	-
C_{15}	-0.9 ± 0.2	-1.0 ± 0.1	-
C_{16}	0.0 ± 1.0	1.0 ± 1.0	-
C_{23}	5.7 ± 0.6	5.0 ± 1.0	-
C_{24}	0.6 ± 0.2	0.6 ± 0.2	-
C_{25}	-0.5 ± 0.3	-0.5 ± 0.2	-
C_{26}	2.0 ± 0.8	1.0 ± 1.0	-
C_{34}	-0.1 ± 0.4	0.2 ± 0.3	-
C_{35}	-0.3 ± 0.2	-0.4 ± 0.1	-
C_{36}	-1.0 ± 0.5	-0.4 ± 0.7	-
C_{45}	0.01 ± 0.04	0.1 ± 0.2	-
C_{46}	-0.5 ± 0.1	0.3 ± 0.2	-
C_{56}	0.1 ± 0.1	0.4 ± 0.1	-

4.3.2 PETN

PETN adopts a comparatively high symmetry tetragonal unit cell containing two molecules. Its space group is $P\bar{4}2_1c$ which belongs to the point group $\bar{4}2m$.^[106] Hence, PETN has 6 independent elastic constants.^[107]

The elastic constants of PETN have been computed at finite temperature using Parrinello-Rahman method in a combined molecular dynamics and Monte Carlo scheme by Borodin *et al.*^[108] Elements of the tensor of elastic constants have also been computed using regular and dispersion-corrected implementations density functional theory at zero and finite temperature by Zhao *et al.*^[109], Conroy *et al.*^[110], and Valenzano *et al.*^[103] Large discrepancies are seen in the three sets of elastic constants computed using density functional theory. This is surprising given the relative simplicity of the PETN unit cell, that all three groups used the strain energy approach, and that both Zhao *et al.* and Conroy *et al.* employed plane wave basis sets with the PBE exchange-correlation functional. The computed sets and sub-sets of elastic constants are presented with the experimental determination by Sun *et al.*^[40] in Table 6.

Table 6. Single crystal elastic constants of PETN in GPa derived from an empirical, non-reactive interatomic potential using the Parrinello-Rahman method,^[108] density functional theory,^[109, 110] and experiment. The DFT-D constants at 295 K correspond to zero temperature dispersion-corrected density functional theory calculations performed at the room temperature mass density of PETN.^[103]

Elastic constant	Parrinello-Rahman, 300 K ^[108]	DFT (PBE GGA), 0 K ^[109]	DFT (PBE GGA), 0 K ^[110]	DFT-D, 0 K ^[103]	DFT-D, 295 K ^[103]	Experiment ^[40]
C_{11}	17.6 ± 0.2	10.1	18.4	37.5	17.4	17.12
C_{33}	10.5 ± 0.1	6.90	14.2	27.2	11.6	12.18
C_{44}	4.66 ± 0.03	-	-	10.3	4.2	5.03
C_{66}	4.92 ± 0.03	-	-	3.7	2.6	3.81
C_{12}	4.7 ± 0.1	-	-	10.2	4.6	6.06
C_{13}	6.65 ± 0.1	-	-	19.4	7.8	7.98

4.3.3 HMX

The 13 independent elastic constants of HMX have been evaluated experimentally and theoretically using a spectrum of methods. Sewell *et al.* ^[71] computed the tensor of elastic constants at room temperature using a combined molecular dynamics and Monte Carlo formalism with the Parrinello-Rahman method and the Smith-Bharadwaj non-reactive force field for nitramines.^[72] More recently Peng *et al.* ^[111] reported the computation of the elastic constants of HMX via dispersion-corrected density functional theory (DFT-D2) at zero temperature via the strain energy method (Eq. 2). Both sets of computed elastic constants are presented along with the room temperature experimental data of Sun *et al.*^[50] in Table 7. The set of elastic constants predicted by Sewell *et al.* using an empirical force field is in remarkably good agreement with the measurements by Sun *et al.* The zero temperature DFT-D2 calculations generally overestimate the experiment data. It is possible that the discrepancies between the DFT-D2 calculations and experiment arise from the neglect of the thermal softening of the elastic moduli in the former. Experimentally determined elastic constants for HMX have been used to predict anisotropic deformation properties,^[112] and to predict phonon density of states, equation of state, and phase behavior for HMX.^[113] Elasticity of HMX has also been used as a starting point in predictions of the phenomena of anisotropic deformation in pore collapse relevant to hot spot initiation.^[114]

Table 7. The single crystal elastic constants of β -HMX in GPa from combined molecular dynamics and Monte Carlo simulations with the Parrinello-Rahman method at 300 K,^[71] dispersion-corrected density functional theory using the strain energy method at zero temperature,^[111] and experiment.^[50]

Tensor component	Parrinello-Rahman, 300 K ^[71]	Strain energy, DFT- D2 ^[111]	Experiment ^[50]
C_{11}	22.2 ± 0.3	29.3	20.58
C_{22}	23.9 ± 0.5	25.0	19.69
C_{33}	23.4 ± 0.5	27.5	18.24
C_{44}	9.2 ± 0.2	13.6	9.92
C_{55}	11.1 ± 0.1	12.8	7.69
C_{66}	10.1 ± 0.1	13.9	10.67
C_{12}	9.6 ± 0.7	10.6	9.65
C_{13}	13.2 ± 0.3	13.8	9.75
C_{15}	-0.1 ± 0.3	-2.1	-0.61
C_{23}	13.0 ± 0.2	16.6	12.93
C_{25}	4.7 ± 0.2	6.2	4.89
C_{35}	1.6 ± 0.2	1.1	1.57
C_{46}	2.5 ± 0.3	6.8	4.42

4.3.4 γ -RDX

γ -RDX is a polymorph of RDX that is stable under hydrostatic pressure in excess of 4 GPa at room temperature.^[115] Like α -RDX it has an orthorhombic unit cell but with space group $Pca2_1$ rather than $Pbca$.^[94, 116] The physical properties of the high pressure phases of energetic materials can potentially control effect impact sensitivity if the principal Hugoniot crosses those phase boundaries. The simulation methods described in the previous sections enable the computation of the single crystal elastic constants of phases stable only at elevated pressures. The molecular dynamics techniques also enable the evaluation of elastic constants at elevated pressures and temperatures.

The elastic constants of γ -RDX were computed under hydrostatic pressures spanning 4 to 11 GPa and temperatures from 200 to 550 K using the Smith-Bharadwaj force field by Munday *et al.*^[65] and Josyula *et al.*^[117] Both works employed identical implementations of the direct method, Eq. 3. Taylor also computed the elastic constants of γ -RDX via dispersion corrected density functional theory (DFT-D3) at zero temperature in the pressure interval 4 to 8 GPa.^[90] The accord between the molecular dynamics simulations and dispersion-corrected density functional theory calculations is generally good.

5 Conclusions

Solid mechanics of explosives is fundamental to predictions of mechanical response and the following chemical response that can result from thermomechanical stimuli. It remains a difficult task to link mechanisms directly to initiation pathways. However, the fundamental mechanics are still of primary importance for many reasons. In this article we have shown that the persistence of many researchers has made far greater precision available in elastic properties through

experimentation and simulation. These properties are precursors for subsequent dynamic material behaviors. The availability of many measurements makes it possible to evaluate the origins of differences and limits of accuracy of fundamental property measurements, and the influence upon predictions.

In this review we have summarized the elastic properties, which is only the initial stage of mechanical deformation, but has proven to be a significant challenge in experiments and simulations. The simplicity of Hooke's Law as a starting point is beguiling. The complexity of explosive materials is formidable. Moving beyond structure determination, understanding of basic elastic deformation requires considerable effort for both experiment and simulation. The materials phenomena between elasticity and hydrodynamics is a subject for a subsequent review. Deformation in the plastic regime, to hydrodynamics and initiation, requires a firm foundation in structure and elasticity, and is further complicated in many other ways. A translated quotation from the 1759 writings of mathematician Alexis Clairaut, discussed by many in reference to the dispute between Newton and Hooke over the originator of the ideas of gravitation, seems apt: "what a distance there is between a truth glimpsed and a truth that is demonstrated."^[e]

Acknowledgements

^e This is described in more detail in the Wikipedia article on Robert Hooke, at http://en.wikipedia.org/wiki/Robert_Hooke. Discussion of this quotation is described in a footnote, reproduced here: "The original statements by Clairaut (in French) are found (with orthography here as in the original) in "Explication abrégée du système du monde, et explication des principaux phénomènes astronomiques tirée des Principes de M. Newton" (1759), at Introduction (section IX), page 6: "Il ne faut pas croire que cette idée ... de Hook diminue la gloire de M. Newton", [and] "L'exemple de Hook" [serves] "à faire voir quelle distance il y a entre une vérité entrevue & une vérité démontrée"."

We are grateful to many we have worked with and discussed with over the years, including, Ralph Menikoff, Tommy Sewell, Lewis Stevens, James Haycraft, Albert Migliori, Betsy Rice, Keith Nelson, Baolian Sun, Jeremy Johnson, Yogi Gupta, Ron Armstrong, and Mitchell Wood.

References

- [1] R. Hooke, in *Lectiones Cutlerianae, or a Collection of Lectures: Physical, Mechanical, Geographical, & Astronomical* (Ed.: R. Hooke), Royal Society, London, **1678**.
- [2] T. Young, *Course of Lectures on Natural Philosophy and the Mechanical Arts*, Taylur and Walton, London, **1845**.
- [3] F. P. Bowden, M. F. R. Mulcahy, R. G. Vines, A. Yoffe, *Proceedings of the Royal Society of London. Series A. Mathematical and Physical Sciences* **1947**, 188, 291.
- [4] F. P. Bowden, M. A. Stone, G. K. Tudor, *Proceedings of the Royal Society of London. Series A. Mathematical and Physical Sciences* **1947**, 188, 329.
- [5] F. P. Bowden, O. A. Gurton, *Proceedings of the Royal Society of London. Series A. Mathematical and Physical Sciences* **1949**, 198, 337.
- [6] F. P. Bowden, M. M. Chaudhri, *Nature* **1968**, 220, 690.
- [7] J. T. M. Dehossion, V. Vitek, *Philosophical Magazine a-Physics of Condensed Matter Structure Defects and Mechanical Properties* **1990**, 61, 305.
- [8] Y. B. Zel'dovich, *Zh. Eksp. Teor. Fiz* **1940**, 10, 542.
- [9] J. von Neumann, in *John von Neumann: Collected Works, 1903-1957, Vol. 6* (Ed.: A. H. Taub), Pergamon Press, New York, **1963**.
- [10] W. Doering, *Annalen der Physik* **1943**, 43, 421.
- [11] R. Menikoff, B. J. Plohr, *Reviews of Modern Physics* **1989**, 61, 75.
- [12] R. Menikoff, *Combustion Theory and Modelling* **2007**, 12, 73.
- [13] R. Menikoff, T. D. Sewell, *Combustion Theory and Modelling* **2002**, 6, 103.
- [14] R. Menikoff, T. D. Sewell, *High Pressure Research* **2001**, 21, 121.
- [15] J. J. Dick, *Applied Physics Letters* **1984**, 44, 859.
- [16] J. J. Dick, *Journal of Applied Physics* **1997**, 81, 601.
- [17] J. J. Dick, D. E. Hooks, R. Menikoff, A. R. Martinez, *Journal of Applied Physics* **2004**, 96, 374.
- [18] J. J. Dick, J. P. Ritchie, *Journal of Applied Physics* **1994**, 75, 2728.
- [19] R. M. Doherty, S. W. Duncan, *Propellants, Explosives, Pyrotechnics* **2008**, 33, 4.
- [20] Z. A. Dreger, Y. M. Gupta, *Journal of Physical Chemistry B* **2007**, 111, 3893.
- [21] R. W. Armstrong, *Central European Journal of Energetic Materials* **2005**, 2, 55.
- [22] R. W. Armstrong, C. S. Coffey, W. L. Elban, *Acta Metallurgica* **1982**, 30, 2111.
- [23] L. Borne, J. Mory, F. Schlessler, *Propellants, Explosives, Pyrotechnics* **2008**, 33, 37.
- [24] M. J. Cawkwell, K. J. Ramos, D. E. Hooks, T. D. Sewell, *Journal of Applied Physics* **2010**, 107, 063512.
- [25] N. C. Dang, Z. A. Dreger, Y. M. Gupta, D. E. Hooks, *The Journal of Physical Chemistry A* **2010**, 114, 11560.
- [26] D. E. Hooks, K. J. Ramos, in *The Thirteenth International Symposium on Detonation*, **2006**.
- [27] D. E. Hooks, K. J. Ramos, A. R. Martinez, *Journal of Applied Physics* **2006**, 100, 024908.
- [28] K. J. Ramos, M. J. Cawkwell, C. A. Bolme, D. E. Hooks, in *15th International Detonation Symposium, Vol. in Press* (Eds.: J. R. Carney, J. L. Maienschein), **2014**.

- [29] K. J. Ramos, D. E. Hooks, T. D. Sewell, M. J. Cawkwell, *Journal of Applied Physics* **2010**, *108*, 066105.
- [30] S. N. Luo, B. J. Jensen, D. E. Hooks, K. Fezzaa, K. J. Ramos, J. D. Yeager, K. Kwiatkowski, T. Shimada, *Review of Scientific Instruments* **2012**, *83*, 073903.
- [31] B. J. Jensen, S. N. Luo, D. E. Hooks, K. Fezzaa, K. J. Ramos, J. D. Yeager, K. Kwiatkowski, T. Shimada, D. M. Dattelbaum, *AIP Advances* **2012**, *2*, 012170.
- [32] H. W. Sandusky, B. C. Beard, B. C. Glancy, W. L. Elban, R. W. Armstrong, *Material Science Research Society Symposium Proceedings* **1993**, *296*, 93.
- [33] L. E. Malvern, *Introduction to the Mechanics of a Continuous Medium*, Prentice-Hall, Inc., Upper Saddle River, NJ, **1969**.
- [34] J. Vial, D. Picart, P. Bailly, F. Delvare, *Modelling and Simulation in Materials Science and Engineering* **2013**, *21*, 045006.
- [35] J. C. Gump, S. M. Peiris, *Journal of Applied Physics* **2005**, *97*, 053513.
- [36] R. Menikoff, Personal Communication, **2014**
- [37] P. J. Rae, D. E. Hooks, C. Liu, in *13th International Detonation Symposium* Norkfolk, VA, **2006**.
- [38] J. J. Haycraft, L. L. Stevens, C. J. Eckhardt, *Journal of Chemical Physics* **2006**, *124*, 024712.
- [39] L. L. Stevens, C. J. Eckhardt, *J. Chem. Phys.* **2005**, *122*, 174701.
- [40] B. Sun, J. M. Winey, N. Hemmi, Z. A. Dreger, K. A. Zimmerman, Y. M. Gupta, D. H. Torchinsky, K. A. Nelson, *Journal of Applied Physics* **2008**, *104*, 073517.
- [41] H. Z. Cummins, P. E. Schoen, in *Laser Handbook* (Eds.: F. T. Arecchi, E. O. Schulz-Dubois), North-Holland Publ. Co. , North-Holland, Amsterdam, **1972**, p. 1029.
- [42] A. Migliori, J. L. Sarrao, W. M. Visscher, T. M. Bell, M. Lei, Z. Fisk, R. G. Leisure, *Physica B* **1993**, *183*, 1.
- [43] K. A. Nelson, M. D. Fayer, *J. Chem. Phys.* **1980**, *72*, 5202.
- [44] I. L. Fabelinskii, *Molecular Scattering of Light*, Plenum, New York, **1968**.
- [45] C. E. Morris, in *Sixth Symposium (International) on Detonation* (Ed.: D. J. Edwards), Office of Naval Research, Arlington, VA, **1976**, pp. 396.
- [46] J. M. Winey, Y. M. Gupta, *J. Appl. Phys.* **2001**, *90*, 1669.
- [47] S. Haussühl, *Z. Kristallogr.* **2001**, *216*, 339.
- [48] R. B. Schwarz, D. E. Hooks, J. J. Dick, J. I. Archuleta, A. R. Martinez, *J. Appl. Phys.* **2005**, *98*, 056106.
- [49] J. J. Haycraft, L. L. Stevens, C. J. Eckhardt, *J. Chem. Phys.* **2006**, *124*, 024712.
- [50] B. Sun, J. M. Winey, Y. M. Gupta, D. E. Hooks, *J. Appl. Phys.* **2009**, *106*, 053505.
- [51] J. M. Zaug, in *Eleventh International Detonation Symposium*, Office of Naval Research, Arlington, VA, **1998**, pp. 498.
- [52] L. L. Stevens, D. E. Hooks, A. Migliori, *Journal of Applied Physics* **2010**, *108*, 053512.
- [53] J. A. Johnson, K. J. Manke, D. G. Veysset, A. A. Maznev, K. J. Ramos, D. E. Hooks, K. A. Nelson, *Journal of Applied Physics* **2011**, *110*, 113513.
- [54] C. A. Bolme, K. J. Ramos, *Journal of Applied Physics* **2014**, *116*, 183503.

- [55] J. J. Haycraft, *Inelastic scattering investigations of vibrational and lattice interactions of the energetic material RDX*, University of Nebraska - Lincoln, Lincoln, NE, **2005**.
- [56] L. L. Stevens, *Intermolecular interactions and dynamics in the solid state: An analysis of beta-HMX*, University of Nebraska - Lincoln, Lincoln, NE, **2005**.
- [57] D. J. Weidner, H. R. Carleton, *Journal of Geophysical Research* **1977**, 82, 1334.
- [58] M. P. Allen, D. J. Tildesley, *Computer Simulation of Liquids*, Oxford University Press, Oxford, **1987**.
- [59] M. W. Finnis, *Interatomic Forces in Condensed Matter*, Oxford University Press, Oxford, **2003**.
- [60] J. H. Henkel, *Journal of Chemical Physics* **1955**, 23, 681.
- [61] M. J. Mehl, J. E. Osburn, D. A. Papaconstantopoulos, B. M. Klein, *Physical Review B* **1990**, 41, 10311.
- [62] A. P. Sutton, T. N. Todorov, M. J. Cawkwell, J. Hoekstra, *Philosophical Magazine a-Physics of Condensed Matter Structure Defects and Mechanical Properties* **2001**, 81, 1833.
- [63] P. Ravindran, L. Fast, P. A. Korzhavyi, B. Johansson, J. Wills, O. Eriksson, *Journal of Applied Physics* **1998**, 84, 4891.
- [64] M. Sob, L. G. Wang, V. Vitek, *Materials Science and Engineering a-Structural Materials Properties Microstructure and Processing* **1997**, 234, 1075.
- [65] L. B. Munday, P. W. Chung, B. M. Rice, S. D. Solares, *Journal of Physical Chemistry B* **2011**, 115, 4378.
- [66] M. Parrinello, A. Rahman, *Journal of Applied Physics* **1981**, 52, 7182.
- [67] M. Parrinello, A. Rahman, *Journal of Chemical Physics* **1982**, 76, 2662.
- [68] M. Sprik, R. W. Impey, M. L. Klein, *Physical Review B* **1984**, 29, 4368.
- [69] J. F. Nye, *Physical Properties of Crystals*, Oxford University Press, Oxford, **1957**.
- [70] M. Karimi, G. Stapay, T. Kaplan, M. Mostoller, *Modelling and Simulation in Materials Science and Engineering* **1997**, 5, 337.
- [71] T. D. Sewell, R. Menikoff, D. Bedrov, G. D. Smith, *Journal of Chemical Physics* **2003**, 119, 7417.
- [72] G. D. Smith, R. K. Bharadwaj, *Journal of Physical Chemistry B* **1999**, 109, 3570.
- [73] A. D. Becke, *Journal of Chemical Physics* **2014**, 140, 18A301.
- [74] K. Burke, *Journal of Chemical Physics* **2012**, 136, 150901.
- [75] E. F. C. Byrd, B. M. Rice, *Journal of Physical Chemistry C* **2007**, 111, 2787.
- [76] S. Ehrlich, J. Moellmann, W. Reckien, T. Bredow, S. Grimme, *Chemphyschem* **2011**, 12, 3414.
- [77] S. Grimme, *Journal of Computational Chemistry* **2006**, 27, 1787.
- [78] S. Grimme, J. Antony, S. Ehrlich, H. Krieg, *Journal of Chemical Physics* **2010**, 132, 154104.
- [79] S. Grimme, S. Ehrlich, L. Goerigk, *Journal of Computational Chemistry* **2011**, 32, 1456.
- [80] S. Grimme, R. Huenerbein, S. Ehrlich, *Chemphyschem* **2011**, 12, 1258.
- [81] S. Grimme, W. Hujo, B. Kirchner, *Physical Chemistry Chemical Physics* **2012**, 14, 4875.
- [82] W. Hujo, S. Grimme, *Physical Chemistry Chemical Physics* **2011**, 13, 13942.

- [83] W. Hujo, S. Grimme, *Journal of Chemical Theory and Computation* **2011**, 7, 3866.
- [84] U. Zimmerli, M. Parrinello, P. Koumoutsakos, *Journal of Chemical Physics* **2004**, 120, 2693.
- [85] R. Balu, E. F. C. Byrd, B. M. Rice, *Journal of Physical Chemistry B* **2011**, 115, 803.
- [86] J. VandeVondele, M. Krack, F. Mohamed, M. Parrinello, T. Chassaing, J. Hutter, *Computer Physics Communications* **2005**, 167, 103.
- [87] J. P. Perdew, K. Burke, M. Ernzerhof, *Physical Review Letters* **1996**, 77, 3865.
- [88] S. Goedecker, M. Teter, J. Hutter, *Physical Review B* **1996**, 54, 1703.
- [89] C. S. Choi, E. Prince, *Acta Crystallographica B* **1972**, 28, 2857.
- [90] D. E. Taylor, *Journal of Applied Physics* **2014**, 116, 053513.
- [91] G. D. Smith, R. K. Bharadwaj, *Journal of Physical Chemistry B* **1999**, 109, 3570.
- [92] D. Bedrov, C. Ayyagari, G. D. Smith, T. D. Sewell, R. Menikoff, J. M. Zaug, *Journal of Computer-Aided Materials Design* **2001**, 8, 77.
- [93] M. J. Cawkwell, T. D. Sewell, L. Zheng, D. L. Thompson, *Physical Review B* **2008**, 78, 014107.
- [94] M. J. Cawkwell, T. D. Sewell, K. J. Ramos, D. E. Hooks, *Plastic Deformation and Phase Transformations in RDX under Shock Loading (LA-UR-08-01489)*, Los Alamos National Laboratory, **2008**
- [95] S. J. Plimpton, *Journal of Computational Physics* **1995**, 117, 1.
- [96] A. P. Thompson, *NPT Dynamics, Minimization, and Elastic Constants for Triclinic Cells*, **2010**, lammmps.sandia.gov/workshops/Feb10/Aidan_Thompson/Triclinic_LAMMPS_2010.pdf
- [97] T. D. Sewell, C. M. Bennett, *Journal of Applied Physics* **2000**, 88, 88.
- [98] D. C. Sorescu, B. M. Rice, D. L. Thompson, *Journal of Physical Chemistry B* **1997**, 101, 798.
- [99] D. C. Sorescu, B. M. Rice, D. L. Thompson, *Journal of Physical Chemistry A* **1998**, 102, 8386.
- [100] D. C. Sorescu, B. M. Rice, D. L. Thompson, *Journal of Physical Chemistry B* **1998**, 102, 6692.
- [101] D. C. Sorescu, B. M. Rice, D. L. Thompson, *Journal of Physical Chemistry B* **1998**, 102, 948.
- [102] D. Bedrov, O. Borodin, G. D. Smith, T. D. Sewell, D. M. Dattelbaum, L. L. Stevens, *Journal of Chemical Physics* **2009**, 131, 224703.
- [103] L. Valenzano, W. J. Slough, W. F. Perger, *AIP Conference Proceedings* **2012**, 1426, 1191.
- [104] O. U. Ojeda, T. Cagin, *Journal of Physical Chemistry B* **2011**, 115, 12085.
- [105] D. J. Luscher, M. A. Buechler, N. A. Miller, *Modelling and Simulation in Materials Science and Engineering* **2014**, 22, 075008.
- [106] H. H. Cady, A. C. Larson, *Acta Crystallographica B* **1975**, 31, 1864.
- [107] D. C. Wallace, *Thermodynamics of Crystals*, Dover, Mineola, NY, **1998**.
- [108] O. Borodin, G. D. Smith, T. D. Sewell, D. Bedrov, *Journal of Physical Chemistry B* **2008**, 112, 734.

- [109] J. Zhao, J. M. Winey, Y. M. Gupta, W. Perger, in *Shock Compression of Condensed Matter - 2003* (Eds.: M. D. Furnish, Y. M. Gupta, J. W. Forbes), **2004**, p. 429.
- [110] M. W. Conroy, I. I. Oleynik, S. V. Zybin, C. T. White, *Physical Review B* **2008**, *77*, 094107.
- [111] Q. Peng, Rahul, G. Wang, L. Gui-Rong, S. De, *Physical Chemistry Chemical Physics* **2014**, *16*, 19972.
- [112] A. R. Zamiri, S. De, *Propellants, Explosives, Pyrotechnics* **2011**, *36*, 247.
- [113] Y. Long, J. Chen, *Philosophical Magazine* **2014**, *94*, 2656.
- [114] N. R. Barton, N. W. Winter, J. E. Reaugh, *Modelling and Simulation in Materials Science and Engineering* **2009**, *17*, 035003.
- [115] B. Olinger, B. Roof, H. Cady, in *Comportement des Milieux Denses sous Hautes Pressions Dynamiques*, Commissariat a l'Energie Atomique (Paris), **1978**, pp. 3.
- [116] A. J. Davidson, I. D. H. Oswald, D. J. Francis, A. R. Lennie, W. G. Marshall, D. I. A. Millar, C. R. Pulham, J. E. Warren, A. S. Cumming, *Crystal Engineering Communications* **2008**, *10*, 162.
- [117] K. Josyula, Rahul, S. De, *RSC Advances* **2014**, *4*, 41491.